Nano Energy 38 (2017) 518–525

Contents lists available at ScienceDirect

Nano Energy

journal homepage: www.elsevier.com/locate/nanoen

Communication

Type-II hetero-junction dual shell hollow spheres loaded with spatially separated cocatalyst for enhancing visible light hydrogen evolution

Zheng Wang[a], Weiwei Wu[b], Qi Xu[a], Gaoda Li[a], Shuhai Liu[b], Xiaofeng Jia[a], Yong Qin[a,b,*], Zhong Lin Wang[c,d,**]

[a] Institute of Nanoscience and Nanotechnology, School of Physical Science and Technology, Lanzhou University, Lanzhou 730000, China
[b] School of Advanced Materials and Nanotechnology, Xidian University, 710071, China
[c] Beijing Institute of Nanoenergy and Nanosystems, Chinese Academy of Sciences, National Center for Nanoscience and Technology (NCNST), Beijing 100083, China
[d] School of Material Science and Engineering, Georgia Institute of Technology, Atlanta, Georgia 30332, USA

ARTICLE INFO

Keywords:
Water splitting
Photocatalyst
Cocatalyst
Type-II hetero-junction
Synergism

ABSTRACT

The solar water splitting performance of a photocatalyst is limited by the recombination of electron-hole pairs and the slow surface catalytic reactions. To conquer these problems, a new kind of Pt/TiO_2/CdS/Co_3O_4 hollow spheres photocatalyst was proposed and synthesized. Its hydrogen evolution rate is 2000 μmol g^{-1} h^{-1} under 100 mW cm^{-2} visible light irradiation, which is over 540 times higher than that of TiO_2/CdS double-shelled hollow spheres under the same conditions. The enhancement can be attributed to the synergistic action between the built-in electric field and spatially separated co-catalysts. This work gives a way to greatly enhance the solar water splitting performance.

1. Introduction

Using the photocatalytic reaction to split water into the clean fuel-hydrogen is one of the most promising routes to solve the energy and environment crisis [1–4]. The typical process of the solar water splitting involves three steps: the generation of electron-hole pairs in the photocatalyst under light illumination, the separation and transportation of charges, and catalyst reaction of charges on the surface. For a given material, the water splitting rate is seriously suppressed by the recombination of the electron-hole pairs and the low surface catalytic reaction speed [5,6]. Therefore, the last two steps are key points in determining the material's water splitting performance [7,8].

As for the second step, constructing type-II hetero-junction and adopting composite structure have been proved to be the effective methods to improve the solar water splitting performance [9,10]. Xie et al. adopted the core-shell CdS/ZnS particle to speed up the water splitting performance [11]; the TiO_2/CdS dual layer 2D materials and the CdS nanoparticle modified TiO_2 nanowires were adopted to enhance the H_2 evolution [12,13]. Each of them indicated that the heterojunction and composite structure improved the separation and transportation of carriers by providing a build-in electric field and optimal transportation path [14].

As for the third step, loading cocatalyst has been proved to be an effective way to speed up the surface catalytic reaction rate as it can reduce the activation energy of reduction and oxidation. Various noble metals, such as Pt and Pd, can enhance the performance by acting as the reduction activity site, while some metal oxides, CoO_x, RuO_2, IrO_2, et al. are capable of improving the oxidation activity [15–18]. Furthermore, loading these two kind cocatalysts onto the photocatalyst simultaneously will further improve the water splitting activity. Domen et al. have demonstrated the efficiency of the structure using a SiO_2/Ta_2O_5 core/shell photocatalyst loaded with Pt NPs on inner and IrO_2 or CoO_x on the outer of the shell [19]; Wang et al. extended this method to the C_3N_4 (a conjugated polymers) [20]. They also demonstrated that the spatially separated cocatalyst will further improve the charges separation and transportation.

As a process containing the last two steps of mutual dependence, the current methods aiming at optimizing individual step are limited in enhancing the water splitting performance. Herein, we designed a double-shelled ultrathin hollow sphere with spatially separated loaded cocatalysts Pt/TiO_2/CdS/Co_3O_4 to enhance the water splitting performance by optimizing the last two steps in the meantime. Such design contributes to 500 times enhancement on H_2 evolution speed. The

* Corresponding author at: Institute of Nanoscience and Nanotechnology, School of Physical Science and Technology, Lanzhou University, Lanzhou 730000, China.
** Corresponding author at: Beijing Institute of Nanoenergy and Nanosystems, Chinese Academy of Sciences, National Center for Nanoscience and Technology (NCNST), Beijing 100083, China.
E-mail addresses: qinyong@lzu.edu.cn (Y. Qin), zhong.wang@mse.gatech.edu (Z.L. Wang).

http://dx.doi.org/10.1016/j.nanoen.2017.05.046
Received 22 March 2017; Received in revised form 6 May 2017; Accepted 22 May 2017
Available online 01 June 2017

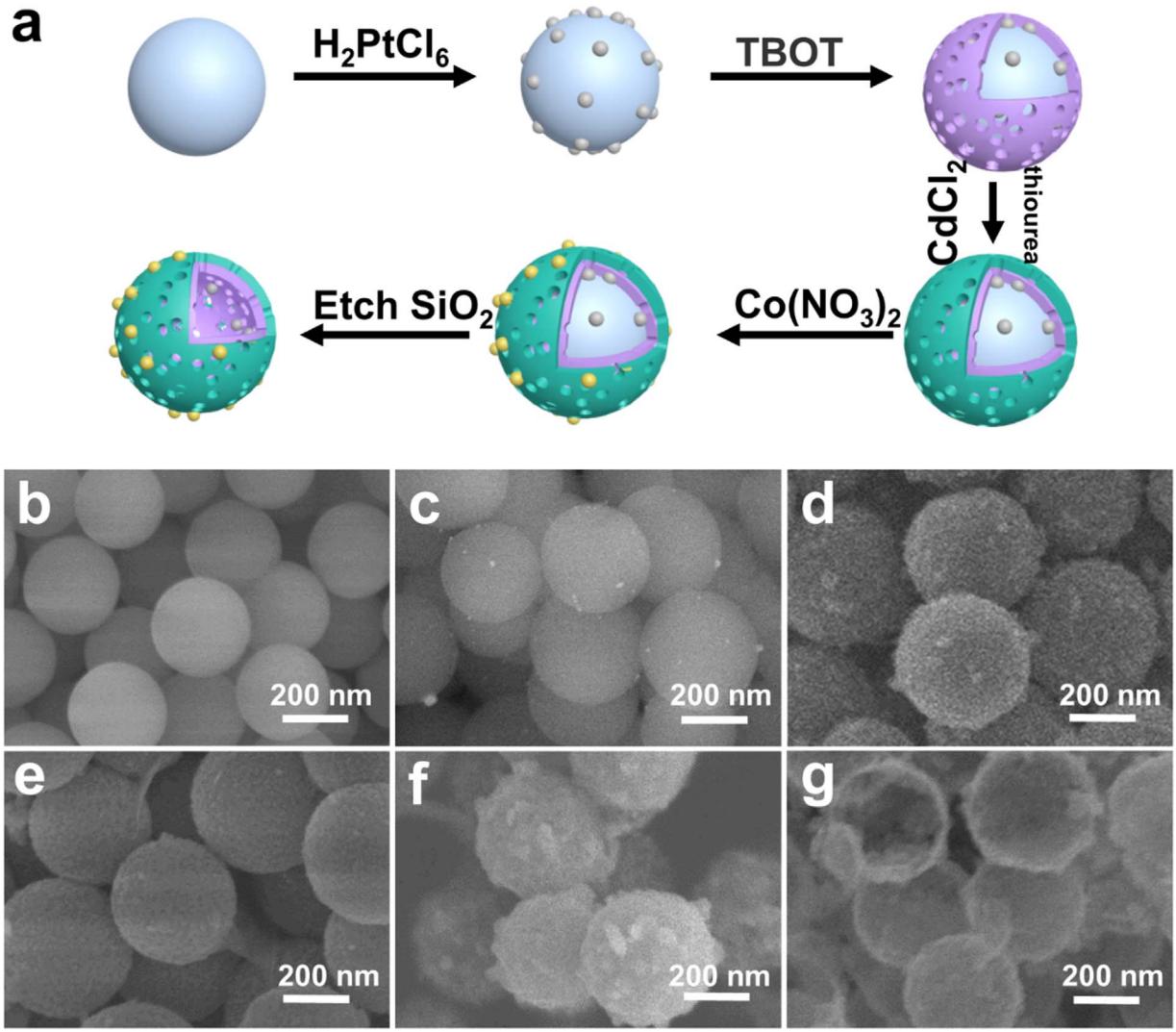

Fig. 1. (a) schematic of the synthesis process of $Pt/TiO_2/CdS/Co_3O_4$ composite hollow spheres; SEM image of (b) SiO_2, (c) Pt loaded SiO_2, (d) $SiO_2/Pt/TiO_2$, (e) $SiO_2/Pt/TiO_2/CdS$ and (f) Co_3O_4 loaded $SiO_2/Pt/TiO_2/CdS$ nanospheres and (g) $Pt/TiO_2/CdS/Co_3O_4$ hollow spheres.

water splitting rate increases from 3.9 μmol g^{-1} h^{-1} (without cocatalyst loaded) to 2000 μmol g^{-1} h^{-1} (with different kinds cocatalysts that are spatially separated loaded) in an aqueous solution containing Na_2S-Na_2SO_3 sacrificial agent under 100 mW cm^{-2} visible light.

2. Experimental methods

2.1. Synthesis of SiO_2 and Pt-loaded SiO_2 nanosphere

The well-known Stober method was used to prepare SiO_2 nanospheres. Typically, 100 mL of TEOS was mixed with 50 mL $NH_3{\cdot}H_2O$, 50 mL H_2O and 400 mL ethanol, then the mixture was kept at 60 °C for 30 min. The solution was stirred for 6 h at 60 °C, resulting in the formation of white SiO_2 colloidal suspension. The silica particles in suspension were separated through centrifugation and washed three times by ethanol. Then the separated SiO_2 particles were annealing at 800 °C for 3 h in muffle furnace to obtain the core material. To obtain the Pt-loaded SiO_2 nanospheres, the SiO_2 nanosphere was dispersed uniformly in ethanol under ultrasound condition, and then a calculated amount of H_2PtCl_6 ethanol solution was dropped to the uniformly dispersed SiO_2 nanospheres ethanol solution, which was grinded to dry. At last, the product was annealed at 400 °C for 30 min in muffle furnace.

2.2. Synthesis of core/shell TiO_2/SiO_2 and $SiO_2/Pt/TiO_2$

The SiO_2/TiO_2 and $SiO_2/Pt/TiO_2$ core/shell structure were synthesized through a typical hydrothermal method [21]. 0.6 mL tetrabutyl titanate was mixed with 37 mL ethanol, 0.25*g* uniformly dispersed SiO_2 or Pt-loaded SiO_2 and 1*g* DI water. Then the solution was transferred to 40 mL autoclave for hydrothermal reaction at 120 °C for 3 h. The resulted product was collected through centrifugation, and washed with ethanol and dried at 80 °C. After annealing at 500 °C for 120 min in muffle furnace, TiO_2 shell with high crystallinity was coated on the surface of the SiO_2 nanospheres or SiO_2/Pt nanospheres.

2.3. Coating CdS layer on the SiO_2 /TiO_2 and $SiO_2/Pt/TiO_2$

$SiO_2/TiO_2/CdS$ or $SiO_2/Pt/TiO_2/CdS$ was prepared through a simple solution reaction [22]. Uniformly dispersed SiO_2/TiO_2 and $SiO_2/Pt/TiO_2$ were added to 150 mL DI water, then 7.5 mL 0.1 M $CdCl_2$ and 15 mL 0.1 M sulfourea were added in turn to the mixture. The pH value of the solution was controlled between 10.0 and 10.5 at 65 °C using $NH_3{\cdot}H_2O$, and then the reaction was kept in stirring for 1.5 h to promote the reaction of the mixture at the same temperature.

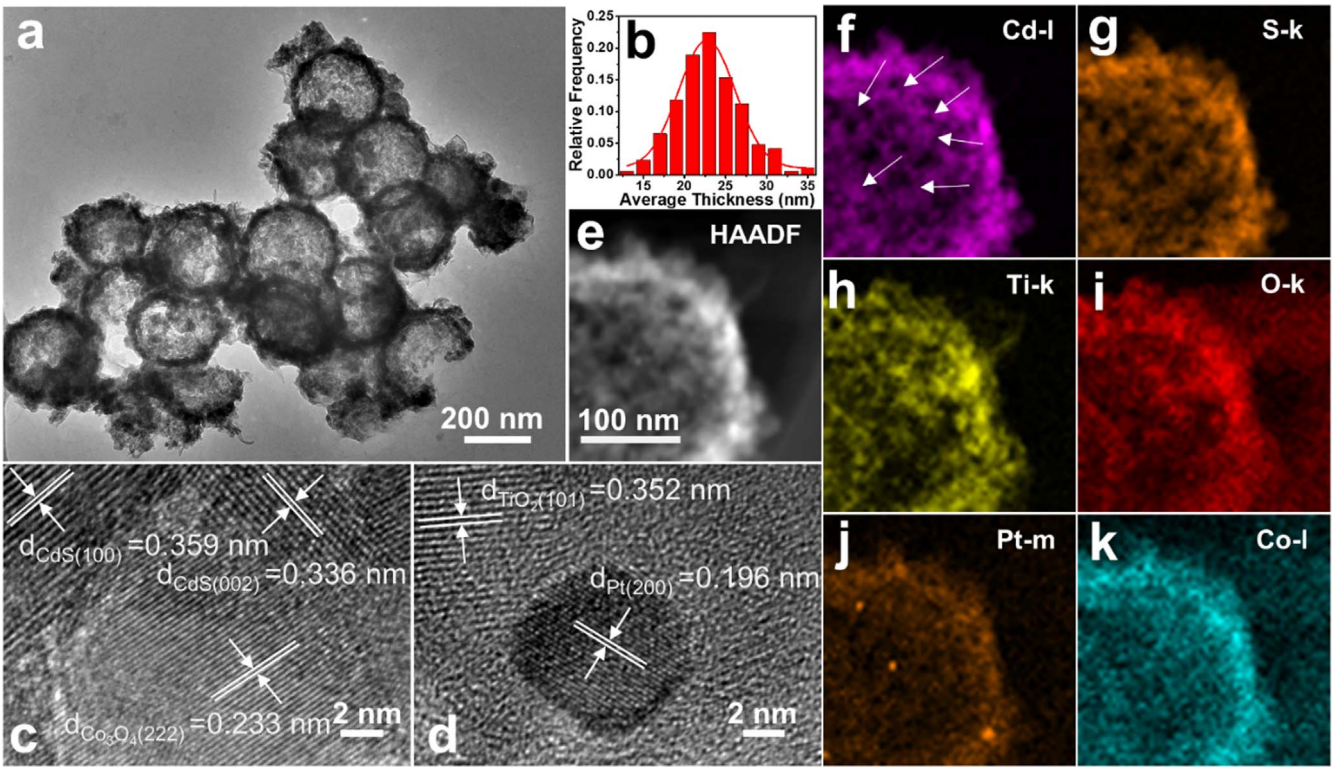

Fig. 2. (a) TEM image of Pt/TiO_2/CdS/Co_3O_4 hollow spheres; (b) the distribution of the hollow spheres thickness; (c) and (d) high resolution TEM image recorded from the wall of the hollow spheres; (e) HAADF-STEM image of the part of a Pt/TiO_2/CdS/Co_3O_4 hollow sphere, and its corresponding elemental maps of (f) Cd, (g) S, (h) Ti, (i) O, (j) Pt and (k) Co.

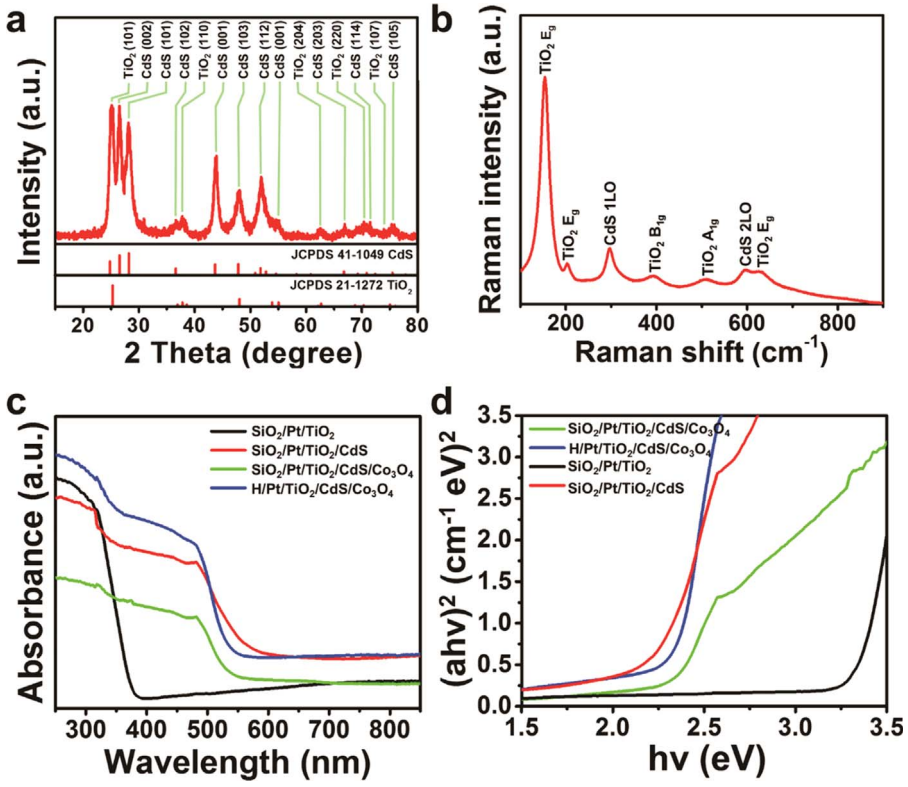

Fig. 3. (a) XRD patterns of Pt/TiO_2/CdS/Co_3O_4 hollowspheres and the JCPDS cards of the CdS and TiO_2; (b) Raman spectra of the Pt/TiO_2/CdS/Co_3O_4 hollowspheres; (c) UV–vis of absorption spectra and (d) the plots of band gap energy of the samples.

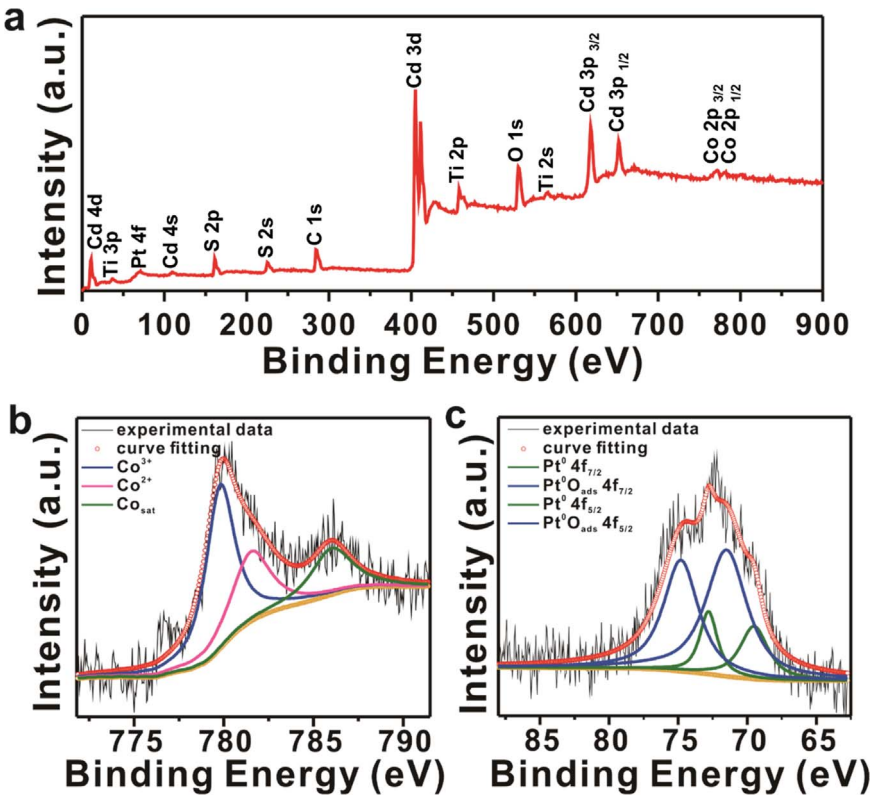

Fig. 4. Fully scanned XPS spectra of (a) $Pt/TiO_2/CdS/Co_3O_4$; high resolution XPS plots of (b) Co $2p_{2/3}$ and (c) Pt 4f.

2.4. Loading Co_3O_4 cocatalysts

The Co_3O_4 cocatalysts were loaded on the surface of $SiO_2/TiO_2/CdS$ or $SiO_2/Pt/TiO_2/CdS$ core/shell through the impregnation method. Typically, a calculated amount of cobalt nitrate was loaded on the surface of $SiO_2/TiO_2/CdS$ and $SiO_2/Pt/TiO_2/CdS$ by evaporated the cobalt nitrate solution. After being annealed at 450 °C in tube furnace with 50 mL min^{-1} Ar flow for 2 h, the Co_3O_4 loaded photocatalysts were obtained.

The hollow spheres were obtained by selectively dissolving SiO_2 core in 10 M NaOH solution at 80 °C for 3 h. The NaOH treated samples were collected through centrifugation and washed with water and dried at 80 °C.

2.5. Basic characterization

The morphology of the hollow spheres photocatlysts were investigated by field emission scanning electron microscope (FE-SEM, Hitachi S-4800), and high resolution transmission electron microscope (HRTEM, Tecnai G2 F30, FEI, USA) equipped with an energy-dispersive X-ray analyzer (EDAX, AMTEK Co., Ltd., USA). Elemental analysis was performed by X-ray photoelectron spectroscope (XPS), which was carried out on Kratos AXIS Ultra DLD XPS instrument equipped with an Al Ka source. X-ray diffraction (XRD) was employed to study the crystallographic of the sample. A Perkin Elmer Lambda 950 spectrometer was used to measure the diffuse reflectance ultraviolet-visible (UV–vis) absorption spectra in the region of 250–850 nm and with $BaSO_4$ as reflectance standard. Raman measurement were carried out using the LabRam HR evolution system using the 532 nm line of an argon ion laser as the excitation source. The cocatalyst loading was detected with an inductively coupled plasma spectrometer (ICP-AES) on an IRIS ER/S instrument (TJA, USA).

2.6. Photocatalytic reaction

The H_2 evolution experiments were carried out in a top-irradiation reaction vessel which was connected to a gas-closed gas circulation system. In a typical reaction, 30 mg of the catalyst powder was dispersed in 0.2 M Na_2S and Na_2SO_3 solution, then the reactant solution was evacuated several times to remove air completely. A commercial solar simulator equipped with a 300 W xenon lamp coupled with a UV cutoff filter ($\lambda > 420$ nm) was used as the light source. The density of the incident light was 100 mW cm^{-2}. The H_2 evolution was measured with an on-line gas chromatograh (GC-7900) equipped with a thermal conductivity detector and the Ar as carrier gas.

3. Result and discussion

Corresponding to the synthesizing illustration in Fig. 1a, each step is characterized via the SEM images from Fig. 1b–g. The surface of the SiO_2 nanospheres is smooth (as shown in Fig. 1b). The loaded Pt nanoparticles are uniformly distributed on the surface of SiO_2 nanospheres, as shown in Fig. 1c where the bright spot are Pt nanoparticles. The subsequent grown TiO_2 and CdS can conformally coat on the Pt loaded SiO_2 nanospheres, as shown in Fig. 1d-e. On the outmost of the core-shell structure, the other kind of cocatalyst Co_3O_4 can also distributed evenly as shown in Fig. 1f. After removing the SiO_2 nanospheres by the NaOH solution, the finally dual shell $Pt/TiO_2/CdS/Co_3O_4$ was obtained with an ultra-thin thickness as shown in Fig. 1g.

The morphology and microstructure of the $Pt/TiO_2/CdS/Co_3O_4$ hollow spheres were further studied by the transmission electron microscopy (TEM). As shown in Fig. 2a and b, the as-prepared $Pt/TiO_2/CdS/Co_3O_4$ hollow spheres are uniform and the average thickness of the shell is 23 nm. The thickness of TiO_2 layer (Fig. S1) is 13 nm. Thus, the thickness of CdS and cocatalyst layer was calculated to be 10 nm which was mainly composed of CdS layer. The high-resolution

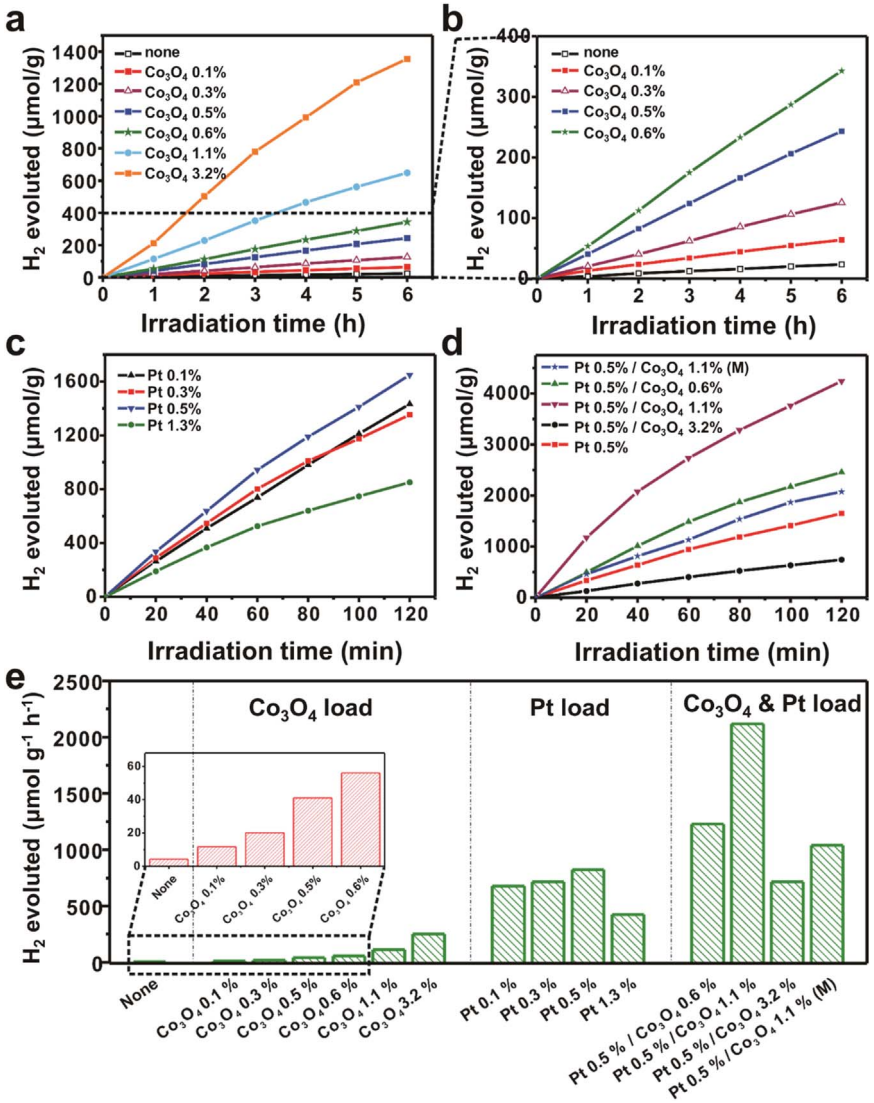

Fig. 5. Hydrogen evolution as a function of time in an aqueous solution containing Na_2S-Na_2SO_3 agent catalyzed by TiO_2/CdS hollow spheres loaded with (a) and (b) Co_3O_4 alone on the outer sphere, (c) Pt alone on the outer sphere and (d) Co_3O_4 and Pt co-catalysts loaded at the same time under 100 mW cm^{-1} visible light irradiation; (e) Hydrogen evolution speed of hollow spheres with different co-catalysts loaded on. The (M) refers to a mixture of Co_3O_4 and Pt, i.e. Co_3O_4 and Pt are not spatially separated.

TEM (HRTEM) of Pt/TiO_2/CdS/Co_3O_4 is shown in Fig. 2c and d. An interplanar spacing of 0.196 nm of the Pt nanoparticle corresponding to the distance between Pt (200) facets (JCPDS card No. 65-2868). The clear lattice fringes with a spacing of 0.233 nm attributed to (222) crystalline plane of Co_3O_4 (JCPDS card No. 43-1003). The shell has clear lattice fringes with interplanar spacing of 0.336 nm and 0.352 nm corresponding to the (002) of CdS (JCPDS card No. 41–1049) and (101) plans of anatase TiO_2 (JCPDS card No. 21–1272), respectively. All of this demonstrates that the TiO_2 and CdS layers possess the high degree of crystallinity. The distribution of each elements in the hollow spheres is further investigated by elemental mapping using high angle annular dark field (HAADF) scanning transmission electron microscopy. As shown in the Fig. 2e-g, the distribution of Cd and S elements is consistent with the morphology shown in HAADF, which further proves that CdS was formed on the external sphere. The distribution of Ti element is different from the morphology shown in HAADF, indicating that TiO_2 was formed on the inner wall. There are no Pt dispersed on the external wall of the TiO_2/CdS hollow spheres, and the distribution of the Co element is similar to the outline of the HAADF. Both the Co_3O_4 and Pt cocatalysts are load on the photocatalyst in particle form rather than shell form, as their contents are rather low in photocatalyst. Combined with the result as shown in Fig. 1c, the TEM results shown in Figs. 2e, j, k, and the synthesis procedure, it can be concluded that the Pt is adhered on the internal wall, and the Co_3O_4 is well dispersed on the external wall of the TiO_2/CdS hollow spheres. In combination of the characterization results and the materials' preparation procedure, it can be verified that the as-prepared hollow spheres were composed of CdS as external layer and TiO_2 as the internal layer while the Pt nanoparticles and Co_3O_4 nanoparticles were separately adhered onto the internal surface of TiO_2 layer and external surface of CdS layer respectively. And the two kinds of nanoparticles are separated by the walls of the hollow spheres.

The crystal phase of the Pt/TiO_2/CdS/Co_3O_4 were clarified by XRD and Raman spectra. As shown in Fig. 3a, all the peaks of the XRD pattern can be indexed to the tetragonal anatase phase TiO_2 (JCPDS card No. 21–1272) and hexagonal CdS (JCPDS card No. 41–1049). The Raman shift spectrum in Fig. 3b exhibits the characteristic bands of anatase TiO_2, i.e, peaks at 395, 517, 153, and 204 cm^{-1}, which can be attributed to the B_{1g}, A_{1g} and E_g modes of anatase TiO_2 [21–23]. The peaks at 300 cm^{-1} and 600 cm^{-1} in the spectrum can be assigned to the first-order longitudinal optic phonon (1LO) and the second-order longitudinal optic phonon (2LO) of CdS respectively [24–26]. So, both of XRD pattern and Raman spectrum prove the hollow spheres are composed of anatase phase TiO_2 and hexagonal CdS, which means

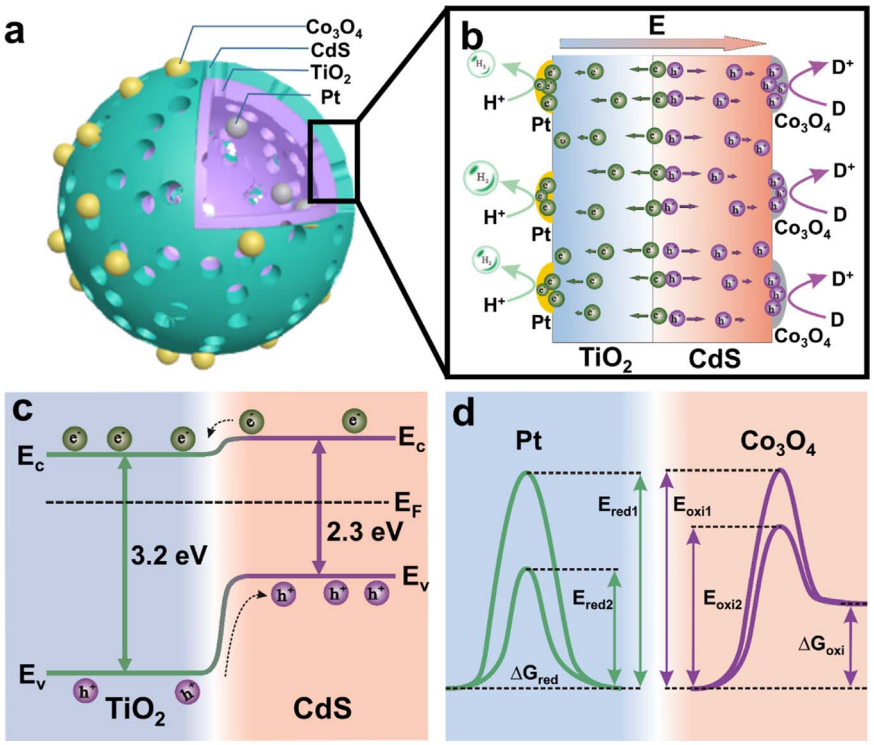

Fig. 6. Illustration of the (a) structure and (b) reaction procedure of double-shelled hollow sphere photocatalyst; Schematic of (c) band structures in TiO_2/CdS double-shelled hollow spheres and (d) activity energy reduction on the surface of photocatalyst with Pt and Co_3O_4 Co-catalyst loaded.

no unwanted chemical reaction occurred in the synthesis even though the sample was annealed at high temperature.

For investigating the optical properties of the photocatalysts, we make a comparison of the UV–vis absorption spectra of the products at different synthesis steps as shown in Fig. 3c and d. The wavelength of TiO_2/Pt/SiO_2's adsorption edge is located at 390 nm, in accordance with the 3.2 eV energy band gap (E_g) for anatase TiO_2. After coating CdS layer, the absorption band of the sample shifts to the visible region wavelength around 540 nm which corresponds to the E_g of 2.3 eV. This absorption property implies that the Pt/TiO_2/CdS/Co_3O_4 hollow spheres has potential in visible-light photocatalysis. The spectrum of Pt/TiO_2/CdS/Co_3O_4 shows a similar light absorption edge with that of TiO_2/CdS, implying no additional band gap transition was induced by the cocatalyst and the light absorbing efficiency of the samples with cocatalyst remain the same.

The chemical composition and valence status of the Pt/TiO_2/CdS/Co_3O_4 were characterized by X-ray photoelectron spectroscopy (XPS). The full scan spectrum shown in Fig. 4a shows the existence of Ti, O, Cd, S, Pt and Co elements in the sample without other impurities. The Co $3d_{3/2}$ and Pt 4 f core level XPS spectra scanned at higher resolution over smaller energy window are shown in Fig. 4b, c. The binding energy peaks at ~780 eV correspond to the Co $2p_{3/2}$. It can be seen that the peak of Co^{3+} locates at 779.9 eV and Co^{2+} at about 781.6 eV after deconvolution, which are in accordance with the presence of Co_3O_4, while an obvious satellite peak at around 786 eV can be attributed to the surface hydroxyl species (i.e. Co-OH) [27–29]. The surface state of the Pt nanoparticles was confirmed by the higher resolution XPS spectrum. As shown in Fig. 4c, Pt 4 f peaks can be divided into two couples of peaks. One couple of the peaks are 69.9 eV and 73.2 eV ascribed to Pt°, while the other couple of peaks are 71.9 eV and 75.2 eV ascribed to $Pt^{\circ}O_{ads}$ ($Pt^{\circ}O_{ads}$ is metallic Pt with surface adsorbed oxygen), both of which are with the typical splitting energy of 13.3 eV [11,30]. The result of the spectrum confirms that the particle adhered on the internal wall of the hollow spheres is the metallic Pt. The Ti 2p, O 1s, Cd 3d and S 2p, core level XPS spectra scanned at higher resolution over smaller energy windows are shown Fig. S2.

The photocatalytic activities of the TiO_2/CdS double-shelled hollow spheres with different kinds of cocatalysts loaded on were evaluated by monitoring hydrogen evolution in an aqueous solution containing Na_2S-Na_2SO_3 as sacrificial agents under 100 mW cm^{-2} visible light irradiation. The plots of H_2 evolution *vs* time of the TiO_2/CdS hollow spheres with different amount of Co_3O_4 loaded on the outer sphere of CdS are shown in Fig. 5a and b. The sample without cocatalyst shows a H_2 evolution rate of 3.9 μmol g^{-1} h^{-1} in 6 h; the rate increases to 10.5 μmol g^{-1} h when 0.1 wt% Co_3O_4 loaded on. With the increase of the loaded amount of Co_3O_4, the H_2 evolution rate of TiO_2/CdS loaded with 3.2 wt% Co_3O_4 reaches 251 μmol g^{-1} h^{-1} which is 64 times higher than that (3.9 μmol g^{-1} h^{-1}) of TiO_2/CdS without cocatalyst. The results show that Co_3O_4 cocatalyst as the holes' collector plays a critical role of enhancing the performance of TiO_2/CdS catalyst. The plots of H_2 evolution vs time of the TiO_2/CdS hollow spheres with different amount of Pt loaded on the TiO_2 inner surface are shown in Fig. 5c. An amount of 0.5 wt% Pt would dramatically enhance the H_2 evolution rate from 3.9 μmol g^{-1} h^{-1} (no cocatalyst loaded on) to 824 μmol g^{-1} h^{-1} in 2 h, which correspond to an increase of almost 210 times. A further increase in the amount of Pt cocatalyst inhibits the H_2 evolution rate instead, as shown in Fig. 5c. Loading either Co_3O_4 or Pt on TiO_2/CdS surfaces can enhance the H_2 evolution rate of catalyst under the same light irradiation. We further evaluated the H_2 evolution performance of Co_3O_4 and Pt loading on the surface of TiO_2/CdS hollow spheres at the same time. For all samples in Fig. 5d, the amount of Pt loaded on the inner sphere is set to 0.5 wt% since this amount leads to the highest performance when only Pt is loaded on. The amount of Co_3O_4 loaded on the outer sphere varies from 0.6 wt% to 1.1 wt% and 3.2 wt%. After the dual cocatalysts (Pt 0.5%/ Co_3O_4 1.1% cocatalysts) were loaded on the TiO_2/CdS, the H_2 evaluation rate reached 2120 μmol g^{-1} h^{-1}, which is 543 higher than that when no cocatalysts are loaded. On the other hand, we also loaded the two kinds of cocatalysts with the same amount randomly on the wall of hollow spheres, indicated in Fig. 5e. As the result shows, the H_2 evolution rate

of sample reaches 1038 μmol g^{-1} h^{-1}, which is higher than that of loading Pt only, but is much lower than that of loading Pt and Co_3O_4 on different spheres. From above discussion, it can be concluded that the synergism between the heterojunction and spatially separated cocatalysts is better than the synergism between the heterojunction and randomly loaded cocatalysts.

The photo-generated carriers' separation, transportation efficiency and interface reaction rate is crucial to the H_2 evaluation rate. The outstanding H_2 evaluation rate (2120 μmol g^{-1} h^{-1}) can be ascribed to the combination of the improved charge's separation, transportation efficiency due to the ultrathin thickness of the dual shell, and increased interface reaction rate due to the synergistic effect of the separately loaded cocatalysts, as shown in Fig. 6a-b. As for a conventional structure with heterojunction, the built-in electric field was created near the junction due to the mismatched Fermi energy levels as shown in Fig. 6c and this electric field usually extend several nanometers near the junction. When this extension distance is comparable with the thickness of the structure, the electric field would exist throughout the structure, in which case the photo-generated electron/holes can be separated and transported efficiently with the assistance of the electric field. The thickness of TiO_2/CdS shell is 23 nm as shown in Fig. 2b, which is comparable with the extension distance of the electric field near the junction, so the charge's separation, transportation efficiency can be improved greatly. With the assistance of built-in electric field, the electrons and holes move toward the TiO_2 and CdS side, respectively. Loading Pt and Co_3O_4 on the surface of the hollow spheres can improve the interface reaction speed as the cocatalysts can decrease the activity energy of the reduction and oxidation reaction in water splitting respectively as shown in Fig. 6d. If Pt and Co_3O_4 were loaded randomly both sides, the Co_3O_4 on TiO_2 side and the Pt on the CdS side have no contribution to the interface reaction rate and even worse, it can induce the reverse reaction of the water splitting. So, loading Pt and Co_3O_4 on TiO_2 and CdS side, respectively, can improve the interface reaction efficiency.

4. Conclusion

In conclusion, the photocatalyst with composite structure had been synthesized and been proved to possess high photo water splitting activity. Such precisely controlled structure, which composed of TiO_2/CdS ultrathin double-shelled hollow spheres and loaded with spatially separated cocatalysts, provides a suitable way to form synergy between the built-in electric field and rapid export charges (activity sites). By rectifying the transportation of the photogenerated charges and maximizing reduction and oxidation reaction, the synergism significantly improves charges separation and transportation and surface reaction in the process of photo water splitting at the same time. The synergistic effect and structure between the heterojunction and spatially separated cocatalyst were designed to improve the activity of the photocatalyst. This benefit to enhancing the efficiency of photo water splitting. And the developed synthesis method can be extended to the general synthesis of nanomaterials with precisely controlled structures.

Acknowledgements

We sincerely appreciate the support from NSFC (NO. 51322203, 51472111), the National Program for Support of Top-notch Young Professionals, the Fundamental Research Funds for the Central Universities (No. lzujbky-2016-k02).

Appendix A. Supporting information

Supplementary data associated with this article can be found in the online version at doi:10.1016/j.nanoen.2017.05.046.

References

[1] F.D. Lin, W.B. Shannon, Nat. Mater. 13 (2014) 81–86.
[2] M.G. Walter, E.L. Warren, J.R. McKone, S.W. Boettcher, Q.X. Mi, E.A. Santori, N.S. Lewis, Chem. Rev. 110 (2010) 6446–6473.
[3] J. Liu, Y. Liu, N.Y. Liu, Y.Z. Han, X. Zhang, H. Huang, Y. Lifshitz, S.T. Lee, J. Zhong, Z.H. Kang, Science 347 (2015) 970–974.
[4] Y. Tachibana, L. Vayssieres, J.R. Durrant, Nat. Photon. 6 (2012) 511–518.
[5] Ariando, X. Wang, G. Baskaran, Z.Q. Liu, J. Huijben, J.B. Yi, A. Annadi, A.R. Barman, A. Rusydi, S. Dhar, Y.P. Feng, J. Ding, H. Hilgenkamp, T. Venkatesan, Nat. Commun. 2 (2011) 188.
[6] A. Kudo, Y. Miseki, Chem. Soc. Rev. 38 (2009) 253–278.
[7] L.C. Mu, Y. Zhao, A.L. Li, S.Y. Wang, Z.L. Wang, J.X. Yang, Y. Wang, T.F. Liu, R.T. Chen, J. Zhu, Energy Environ. Sci. 9 (2016) 2463–2469.
[8] X. Wang, Q. Xu, M. Li, S. Shen, X. Wang, Y. Wang, Z. Feng, J. Shi, H. Han, C. Li, Angew. Chem. Int. Ed. 51 (2012) 13089–13092.
[9] X. Yu, J. Zhang, Z. Zhao, W. Guo, J. Qiu, X. Mou, A. Li, J.P. Claverie, H. Liu, Nano Energy 16 (2015) 207–217.
[10] N.N. Hewa-Kasakarage, P.Z. El-Khoury, A.N. Tarnovsky, M. Kirsanova, I. Nemitz, A. Nemchinov, M. Zamkov, ACS Nano 4 (2010) 1837–1844.
[11] Y.P. Xie, Z.B. Yu, G. Liu, X.L. Ma, H.M. Cheng, Energy Environ. Sci. 7 (2014) 1895–1901.
[12] J. Zhang, Z. Zhu, Y. Tang, K. Müllen, X. Feng, Adv. Mater. 26 (2014) 734–738.
[13] G. Ai, H. Li, S. Liu, R. Mo, J. Zhong, Adv. Funct. Mater. 25 (2015) 5706–5713.
[14] H. Li, Y. Zhou, W. Tu, J. Ye, Z. Zou, Adv. Funct. Mater. 25 (2015) 998–1013.
[15] X. Zong, H.J. Yan, G.P. Wu, G.J. Ma, F.Y. Wen, L. Wang, C. Li, J. Am. Chem. Soc. 130 (2008) 7176–7177.
[16] K. Maeda, K. Domen, J. Phys. Chem. Lett. 1 (2010) 2655–2661.
[17] J. Yang, H. Yan, X. Wang, F. Wen, Z. Wang, D. Fan, C. Li, J. Catal. 290 (2012) 151–157.
[18] K. Maeda, A. Xiong, T. Yoshinaga, T. Ikeda, N. Sakamoto, T. Hisatomi, M. Takashima, D. Lu, M. Kanehara, T. Setoyama, T. Teranishi, K. Domen, Angew. Chem. Int. Ed. 122 (2010) 4190–4193.
[19] D. Wang, T. Hisatomi, T. Takata, C. Pan, M. Katayama, J. Kubota, K. Domen, Angew. Chem. Int. Ed. 52 (2013) 11252–11256.
[20] D. Zheng, X.N. Cao, X. Wang, Angew. Chem. Int. Ed. 55 (2016) 11512–11516.
[21] W. Hu, W. Zhou, K. Zhang, X. Zhang, L. Wang, B. Jiang, G. Tian, D. Zhao, H. Fu, J. Mater. Chem. A 4 (2016) 7495–7502.
[22] Y. Yang, L. Qu, L. Dai, T.S. Kang, M. Durstock, Adv. Mater. 19 (2007) 1239–1243.
[23] W. Zhou, F. Sun, K. Pan, G. Tian, B. Jiang, Z. Ren, C. Tian, H. Fu, Adv. Funct. Mater. 21 (2011) 1922–1930.
[24] J.M. Nel, H.L. Gaigher, F.D. Auret, Thin Solid Films 436 (2003) 186–195.
[25] R.R. Prabhu, M.A. Khadar, Bull. Mater. Sci. 31 (2008) 511–515.
[26] Z. Chen, Y.J. Xu, ACS Appl. Mater. Interfaces 5 (2013) 13353–13363.
[27] S.C. Petitto, M.A. Langell, J. Vac. Sci. Technol. A 22 (2004) 1690–1696.
[28] J. Zhu, K. Kailasam, A. Fischer, A. Thomas, ACS Catal. 1 (2011) 342–347.
[29] K.S. Kim, N. Winograd, R.E. Davis, J. Am. Chem. Soc. 93 (1971) 6296–6297.
[30] R. Nie, J. Shi, W. Du, W. Ning, Z. Hou, F.S. Xiao, J. Mater. Chem. A 1 (2013) 9037–9045.

Zheng Wang received his B.S. degree in Material Chemistry from Lanzhou University , China in 2012. Currently, he is a Ph.D. student in School of Physical Science and Technology of Lanzhou University at Institute of Nanoscience and Nanotechnology. His research mainly focuses on synthesis of nanomaterials and its applications.

Weiwei Wu received his B.S. degree in Material Chemistry (2007) and Ph.D degree in Materials Physics and Chemistry (2014) supervised by Prof. Yong Qin from Lanzhou University, China. Then, he had been a postdoctoral fellow in Technion-Israel Institute of Technology (2015–2016) supervised by Prof. Hossam Haick. Currently he is an associate professor in School of Advanced Materials and Nanotechnology, Xidian University. His research mainly focuses on synthesis of one-dimensional nano-materials and its applications.

Qi Xu received his B.S. in Electronic Device and Materials Engineering from Lanzhou University, China in 2010. Now he is a Ph.D. student in School of Physical Science and Technology of Lanzhou University at Institute of Nanoscience and Nanotechnology. His research mainly focuses on energy harvesting.

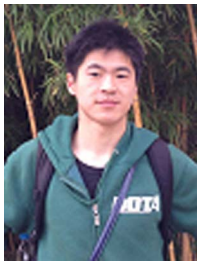

Gaoda Li received his B.S. in Physics from Lanzhou University, China in 2013. Now he is a Ph.D. student in School of Physical Science and Technology of Lanzhou University at Institute of Nanoscience and Nanotechnology. His research mainly focuses on the physical properties influenced by surface chemisorption.

Shuhai Liu received his B.S. (2012) in Applied Physics from Hua Zhong University of Science and Technology and M.S. (2015) in Condensed Matter Physics from University of Chinese Academy of Sciences. From 2015–2017, he worked as an assistant engineer in China Electronics Technology Group Corporation. Now he is a Ph.D student in Professor Yong Qin's group at Xidian University. His research mainly focuses on piezotronics, piezo-phototronics and fundamental physical properties characterization based on atomic force microscopy.

Xiaofeng Jia received his B.S. in Materials Chemistry from Tianjin University of Technology, China in 2013. Now he is a Ph.D. student at the Institute of Nanoscience and Nanotechnology, Lanzhou University. His research mainly focuses on synthesis of two-dimensional materials and fabrication of functional nanodevices.

Yong Qin received his B.S. (1999) in Material Physics and Ph.D. (2004) in Material Physics and Chemistry from Lanzhou University. From 2007–2009, he worked as a visiting scholar and Postdoc in Professor Zhong Lin Wang's group at Georgia Institute of Technology. Currently, he is a professor at the Institute of Nanoscience and Nanotechnology, Lanzhou University, where he holds a Cheung Kong Chair Professorship. His research interests include nanoenergy technology, functional nanodevice and self-powered nanosystem. Details can be found at: http://www.yqin.lzu.edu.cn.

Prof. Zhong Lin Wang received his Ph.D from Arizona State University in physics. He now is the Hightower Chair in Materials Science and Engineering, Regents' Professor, Engineering Distinguished Professor and Director, Center for Nanostructure Characterization, at Georgia Tech. Dr. Wang has made original and innovative contributions to the synthesis, discovery, characterization and understanding of fundamental physical properties of oxide nanobelts and nanowires, as well as applications of nanowires in energy sciences, electronics, optoelectronics and biological science. His discovery and breakthroughs in developing nanogenerators established the principle and technological road map for harvesting mechanical energy from environment and biological systems for powering a personal electronics. His research on self-powered nanosystems has inspired the worldwide effort in academia and industry for studying energy for micro-nano-systems, which is now a distinct disciplinary in energy research and future sensor networks. He coined and pioneered the field of piezotronics and piezo-phototronics by introducing piezoelectric potential gated charge transport process in fabricating new electronic and optoelectronic devices. Details can be found at: www.nanoscience.gatech.edu.